Electronic Supplementary Material (ESI) for ChemComm.

Bimetallic Sulfide $FeCoS_4$@rGO Hybrid as A High-Performance Anode for Potassium-ion Batteries

Erjin Zhang[a], Yuanning Luo[a], Hongwei Fu[b], Zhentao Luo[a], Peng Wang[a], Xuejiao Wang*[a], Li Xu*[a], Huaming Li[a]

a. Institute for Energy Research, School of Mechanical Engineering, Jiangsu University, Zhenjiang 212013, People's Republic of China

b. School of Physics and Electronics, Hunan University, Changsha 410082, People's Republic of China

∗ Corresponding authors. E-mail: wangxuejiao@ujs.edu.cn

Experimental Section

1. Chemicals and materials

The Ferric chloride hexahydrate ($FeCl_3$•6 H_2O), Cobalt chloride hexahydrate ($CoCl_2$•6 H_2O), Sulfur (S, 99.5%), Ammonium hydroxide (NH_3•H_2O), ethanol (EtOH, 99.8%), and graphene oxide (GO) were purchased from Sinopharm Chemical Reagent Co. Ltd., Shanghai, China.

2. Material Preparation

Preparation of $FeCoS_4$@rGO: Initially, 0.5406 g $FeCl_3$•6 H_2O and 0.4758 g $CoCl_2$•6 H_2O were added to the 90 ml deionized water and stir until completely dissolved. Subsequently, 10 ml of NH_3•H_2O was added, and the mixture was stirred at 90 ℃ for 4 hours. After the solution naturally cooled down, the precipitate was collected by centrifugation and dried at 60 ℃ for 12 hours.

0.2 g precursor and 0.2 g sulfur powder were thoroughly mixed in a mortar. Subsequently, the mixture was annealed at 155 ℃ for 2 hours with a heating rate of 5 ℃ min^{-1} under an argon (Ar) atmosphere. The temperature was then increased to 450 ℃ (or alternatively, to 350 ℃, 650 ℃) at the same rate and held for 3 hours. Finally, the bimetallic sulfide $FeCoS_4$ (or $FeCoS_2$) was obtained. $FeCoS_4$@rGO was prepared by adding a solution of 0.75 mg/ml graphene oxide to the precursor solution.

3. Material characterization

Bimetallic sulfide was characterized by field-emission SEM (Tescan Mira4) and

TEM (FEI Talos F200S). X-ray powder diffraction (XRD, XRD 6100 (Cu Kα)) was used to examine the crystal structure of the sample. Raman spectra was obtained by using a confocal Raman microscope system (WITec, alpha 300 R) with a 532 nm wavelength yttrium aluminum garnet (YAG) laser. X-ray photoelectron spectroscopy (XPS) was performed using the Thermo Scientific K-Alpha + from a single anode at 72 W. Thermal gravimetric analysis (TGA) was carried out on a Microcomputer differential thermal balance (HCT-1) under nitrogen atmospheres, respectively.

4. Electrochemical Measurements

The active material was mixed with Ketjen black and carboxymethylcellulose (CMC) binder with mass ratio of 7:2:1 and dissolved in distilled water solvent to produce electrode slurry by continuous agitation for 8 h. The slurry was uniformly pasted onto copper foil current collector. The electrodes were dried in a vacuum oven at 60 °C overnight. CR2032 Coin cells were assembled in glove box (<1 ppm of water and oxygen) with counter electrode (potassium metal) and electrolyte (3M KFSI in DME). The loading mass of active material is about 1.0 mg cm^{-2}. The assembled coin cell was tested at various current densities over the range of 0.01–3.0 V with Neware BTS-8.0.0 battery testing system. CV measurements were performed on a CHI660e electrochemical workstation (Chenhua, Shanghai) at 0.1 mV s^{-1} from 0.01 to 3.0 V.

Galvanostatic Intermittent Titration Technique (GITT) tests were utilized to investigate the reaction kinetics of K ion storage. The experiment employed a current density of 50 mA g^{-1} with a pulse time of 30 minutes, followed by relaxation intervals of equal duration across the entire range of relevant voltages.

5. Calculated method

All the density functional theories (DFT) calculations were conducted based on the Vienna Ab-inito Simulation Package (VASP)[1]. The exchange-correlation effects were described by the Perdew-Burke-Ernzerhof (PBE) functional within the generalized gradient approximation (GGA) method[2]. The core-valence interactions were accounted by the projected augmented wave (PAW) method[3]. The energy cutoff for plane wave expansions was set to 400 eV. The structural optimization was completed for energy and force convergence set at 1.0×10^{-5} eV and 0.02 eV $Å^{-1}$,

respectively. The Brillouin zone was sampled with the 3×3×1 K-point. Grimme's DFT-D3 methodology was used to describe the dispersion interactions[4].

The adsorption energies (Eads) are calculated by:

$E_{ads} = E_{*K} – E_K – E_{Sub}$

where E_K and E_{*K} represent the energies before and after the adsorption of K on the substrate, respectively. E_{sub} is the energy of clean surface.

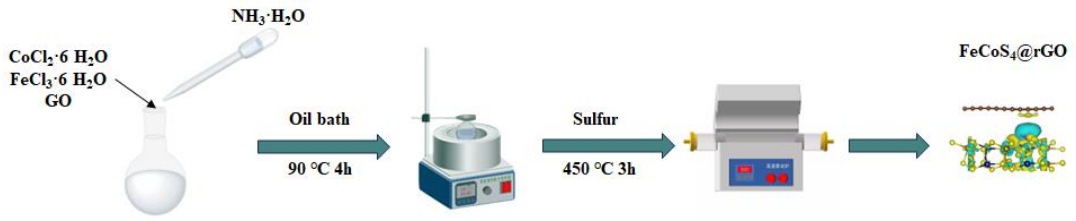

Fig. S1 Schematic illustration of the synthesis process of $FeCoS_4$@rGO.

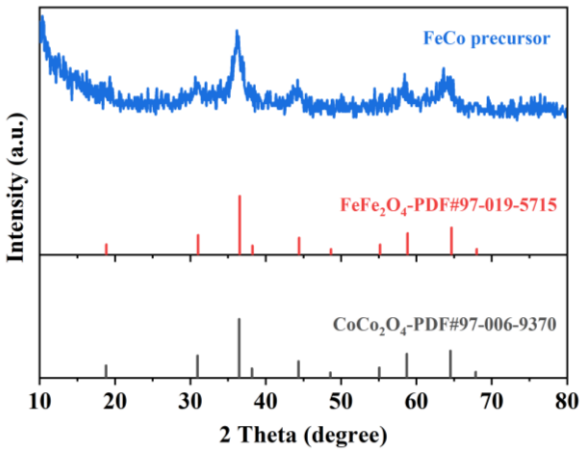

Fig. S2 The XRD spectra of FeCo precursor.

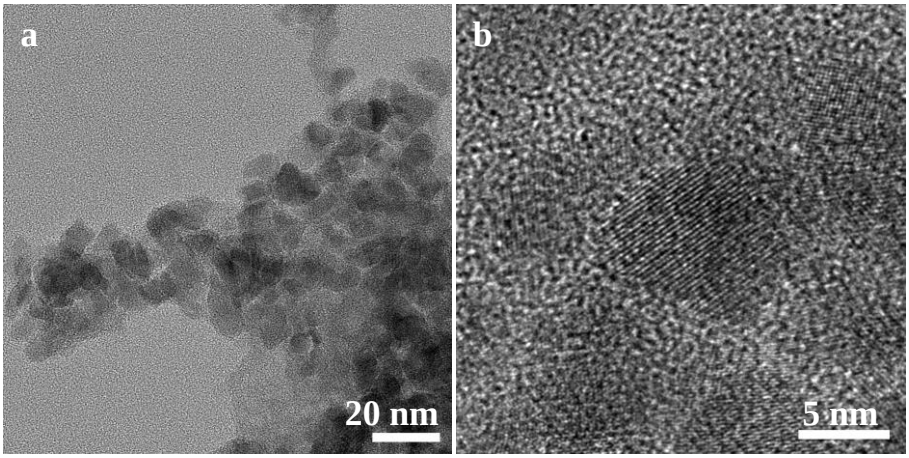

Fig. S3 The TEM of a-$FeCoS_4$ at 350 ℃.

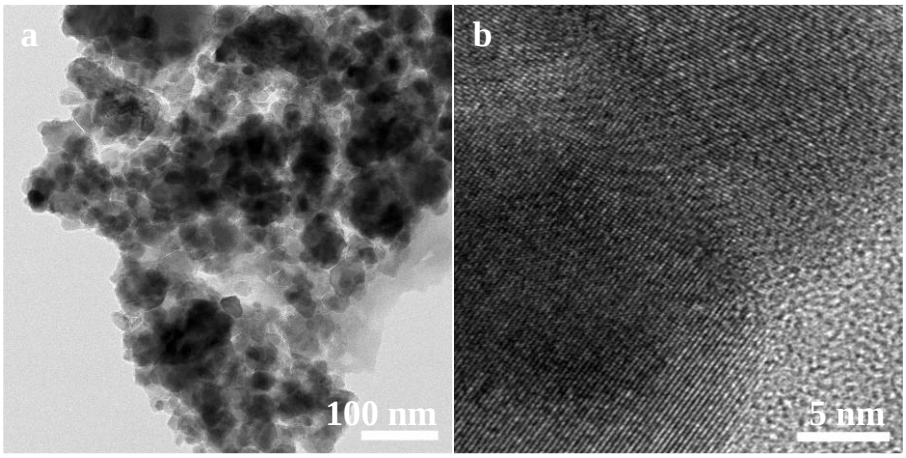

Fig. S4 The TEM of $FeCoS_4$ 450 ℃.

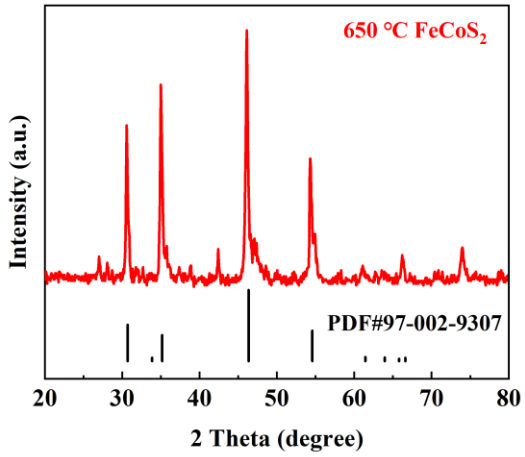

Fig. S5 The XRD spectra of $FeCoS_2$.

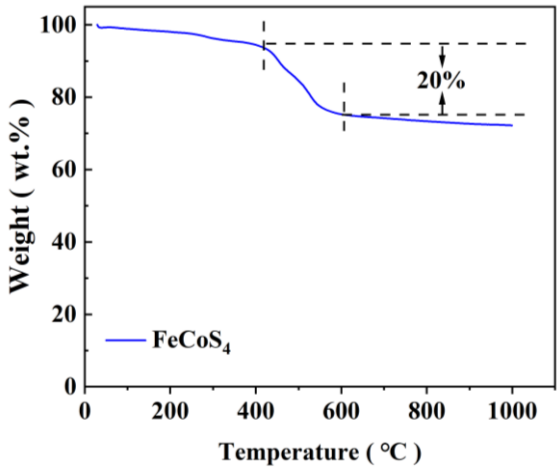

Fig. S6 The thermal gravimetric analysis (TGA) of $FeCoS_4$ in an argon atmosphere.

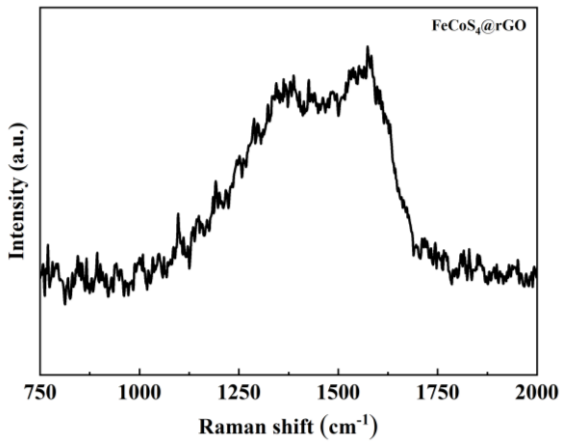

Fig. S7 The Raman spectra of $FeCoS_4$@rGO.

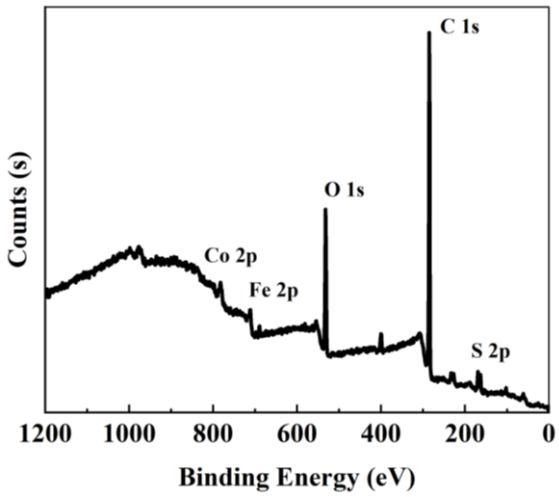

Fig. S8 The XPS full spectrum of $FeCoS_4$@rGO.

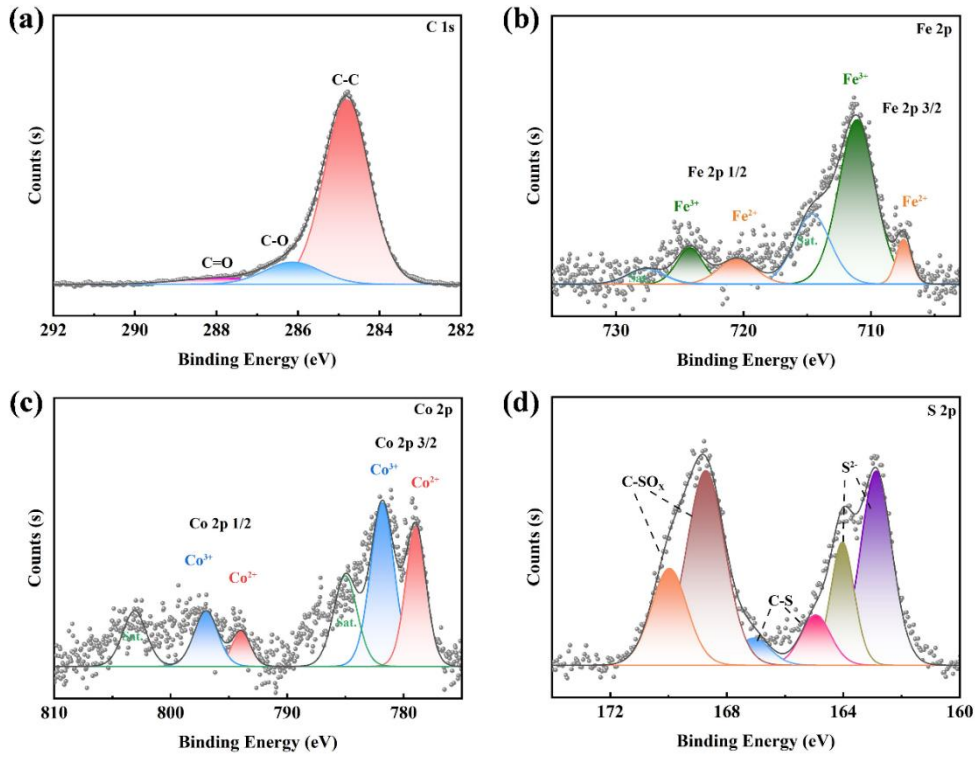

Fig.S9 High-resolution C 1s (a), Fe 2p (b), Co 2p (c), and S 2p (d) XPS spectra of $FeCoS_4$@rGO.

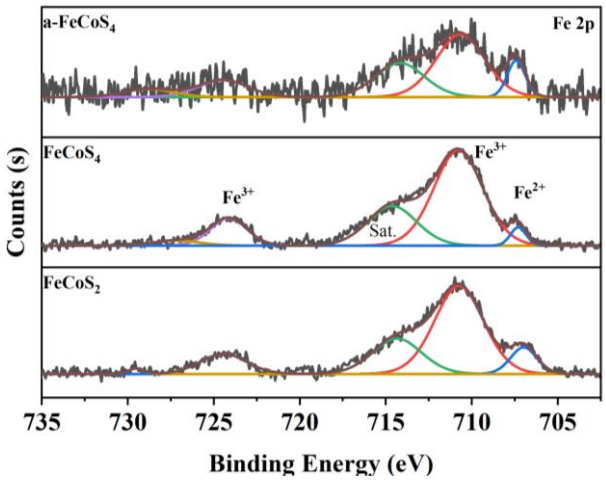

Fig. S10 The high-resolution XPS spectra of Fe 2p in bimetallic sulfides for a-$FeCoS_4$, $FeCoS_4$, and $FeCoS_2$.

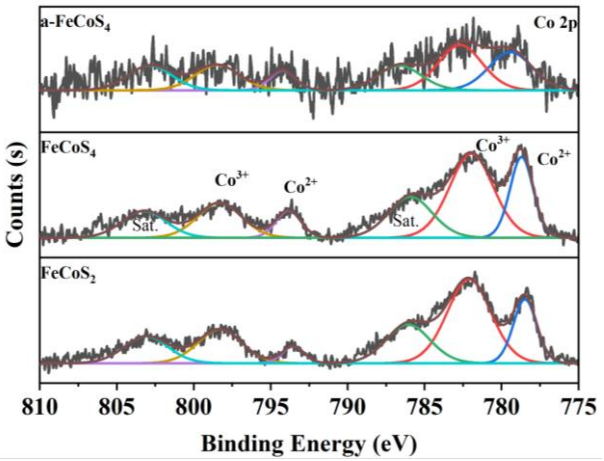

Fig. S11 The high-resolution XPS spectra of Co 2p in bimetallic sulfides for a-$FeCoS_4$, $FeCoS_4$, and $FeCoS_2$.

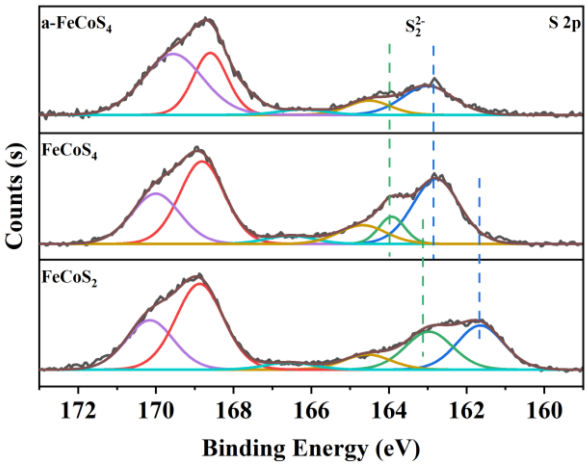

Fig. S12 The high-resolution XPS spectra of S 2p in bimetallic sulfides for a-$FeCoS_4$, $FeCoS_4$, and $FeCoS_2$.

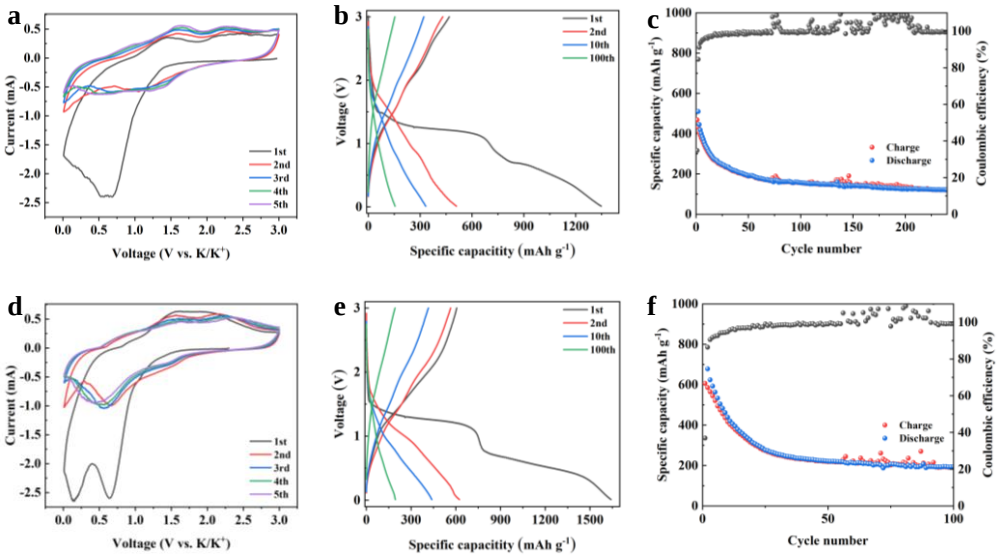

Fig. S13 The CV curves, charge-discharge curves and cycling performance for a-$FeCoS_4$ (a-c) and $FeCoS_2$ (d-f).

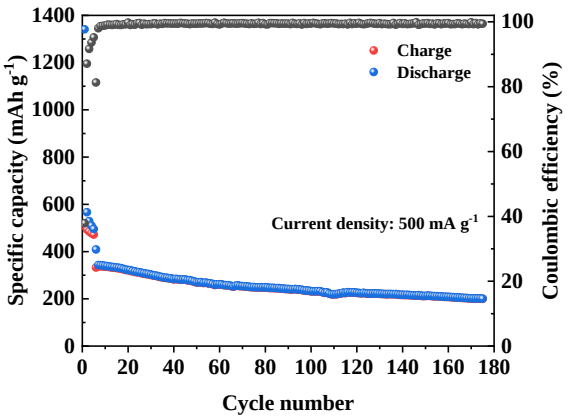

Fig. S14 Cycling performance for $FeCoS_4$@rGO at 500 mA g^{-1}.

Fig. 15 Digital photo of a disassembled battery showing capacity fluctuations during cycling.

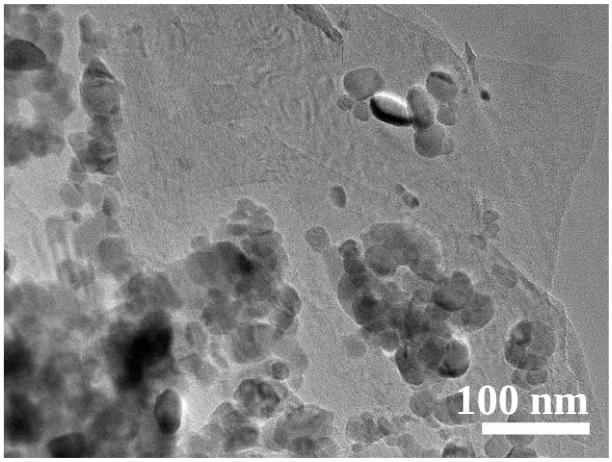

Fig. S16 TEM image of $FeCoS_4$@rGO electrode after 50 cycles.

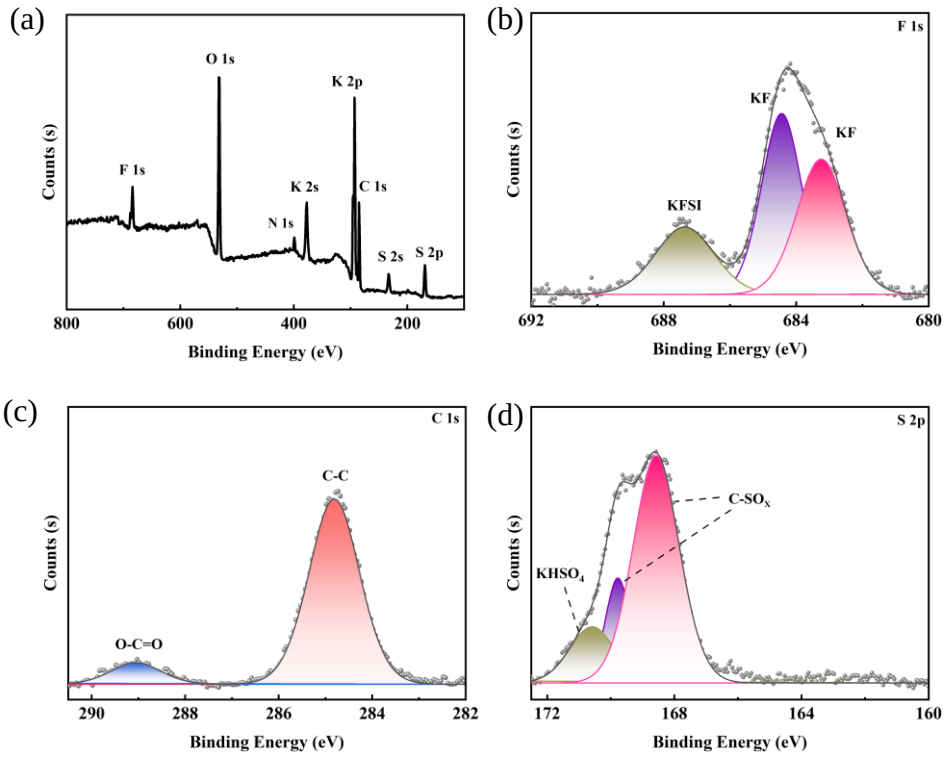

Fig. S17 XPS analysis of $FeCoS_4$@rGO after 10 cycles.

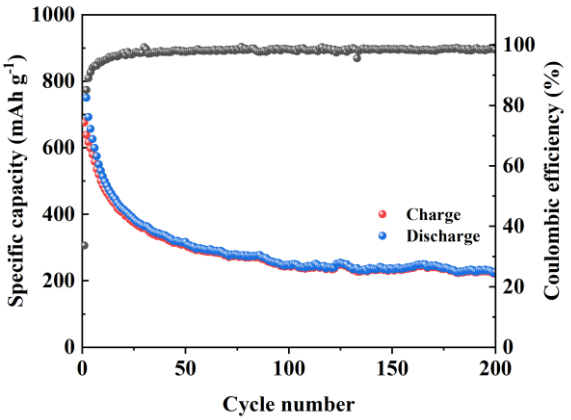

Fig. S18 The cycling performance for $FeCoS_4$ at 50 mA g^{-1}.

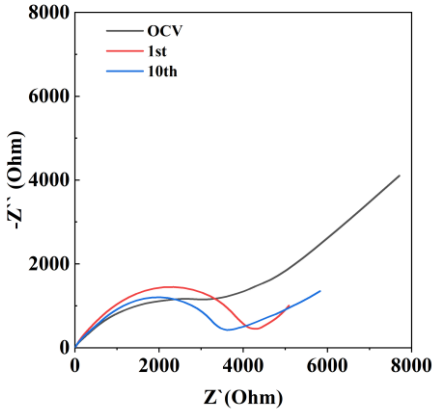

Fig. S19 The EIS plots of $FeCoS_4$ at different states.

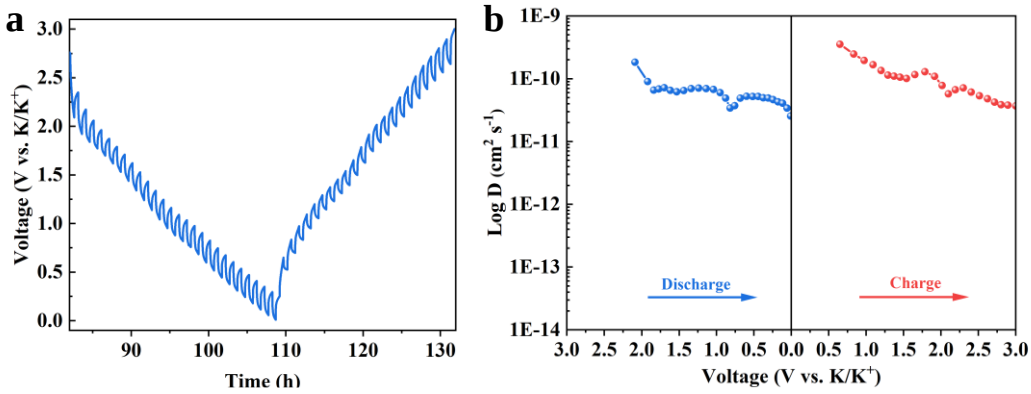

Fig. S20 $D_{K\text{-}ion}$ of $FeCoS_4$@rGO electrodes calculated at different potassiation and de-potassiation process for 2nd cycle.

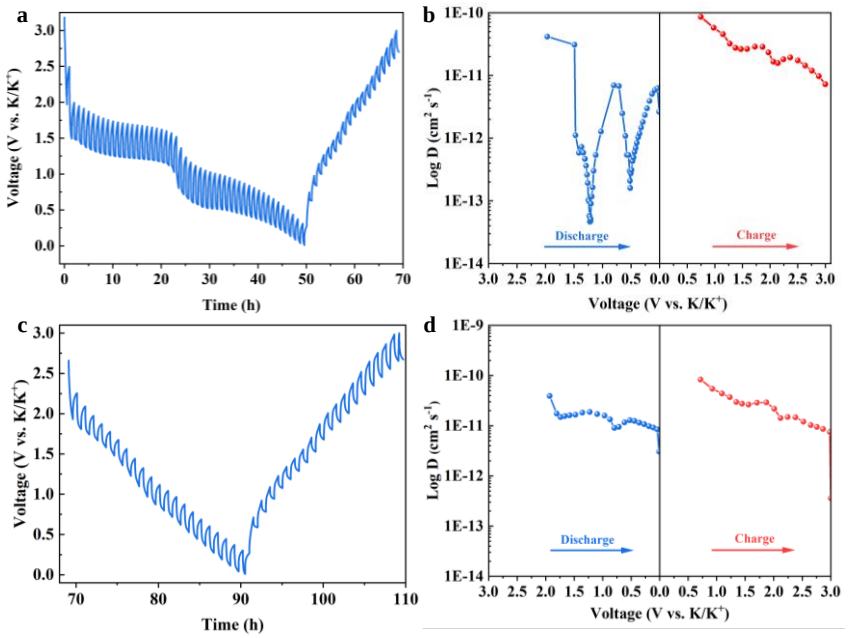

Fig. S21 The time-voltage curve (a and c) and $D_{K\text{-ion}}$ (b and d) of $FeCoS_4$ electrodes for 1st and 2nd cycle.

Table S1 The PIB performance compares with reported results.

Material	Voltage range (V)	Current (mA g^{-1})	Discharge capacity (mAh g^{-1})	Cycle number	Rate capacity (mAh g^{-1})	Ref.
$FeCoS_4$@rGO	0.01-3	50	404	100	246 (1 A g^{-1})	This work
NiS_2/rGO	0.1-2	50	320	100	94 (6.4 A g^{-1})	5
MoS_2@C nanosheets	0.01-3	100	280.6	100	51 (2 A g^{-1})	6
ZnS@C	0.01-3	100	310	100	150 (5 A g^{-1})	7
Ti_3C_2–Sb_2S_3	0.01-2	100	386	500	102 (2 A g^{-1})	8
Co_9S_8/N-C@MoS_2	0.01-3	1000	100	100	100 (1 A g^{-1})	9
GeV_4S_8	0.01-3	200	364.3	100	184 (5 A g^{-1})	10
$FeCoS_2$@rGO	0.01-3	100	371.5	150	182 (2 A g^{-1})	11
SnS@C/rGO	0.3-2	800	176	50	211 (0.8 A g^{-1})	12

References

(1) Kresse, G.; Hafner, J. Ab initio molecular dynamics for liquid metals. *Physical review B* **1993**, *47* (1), 558. Kresse, G.; Hafner, J. Ab initio molecular-dynamics simulation of the liquid-metal–amorphous-semiconductor transition in germanium. *Physical Review B* **1994**, *49* (20), 14251.

(2) Perdew, J. P.; Burke, K.; Ernzerhof, M. Generalized gradient approximation made simple. *Phys. Rev. Lett.* **1996**, *77* (18), 3865.

(3) Blöchl, P. E. Projector augmented-wave method. *Physical review B* **1994**, *50* (24), 17953.

(4) Grimme, S.; Antony, J.; Ehrlich, S.; Krieg, H. A consistent and accurate ab initio parametrization of density functional dispersion correction (DFT-D) for the 94 elements H-Pu. *The Journal of chemical physics* **2010**, *132* (15).

(5) Zheng, H.; Chen, X.; Li, L.; Feng, C.; Wang, S. Synthesis of NiS2/reduced graphene oxide nanocomposites as anodes materials for high-performance Sodium and Potassium ion batteries. *Mater. Res. Bull.* **2021**, *142*. DOI: 10.1016/j.materresbull.2021.111430.

(6) Chen, L.; Chen, Z.; Xiang, T.; Wang, X.; Feng, S.; Yang, S.; Wang, Z.; Feng, Z.; Li, X.; Huang, J. Expanded MoS2@C nanosheets by three-roll milling for high-performance potassium ion batteries. *FlatChem* **2023**, *40*. DOI: 10.1016/j.flatc.2023.100520.

(7) Gan, Y.; Mu, M.; Li, M.; Ma, X.; Yuan, J.; He, H.; Li, X.; Mou, J.; Zhang, C.; Zhang, X.; et al. Trumpet-Like ZnS@C Composite for High-Performance Potassium Ion Battery Anode. *Chemistry* **2023**, *29* (32), e202300373. DOI: 10.1002/chem.202300373.

(8) Wang, T.; Shen, D.; Liu, H.; Chen, H.; Liu, Q.; Lu, B. A Sb(2)S(3) Nanoflower/MXene Composite as an Anode for Potassium-Ion Batteries. *ACS Appl Mater Interfaces* **2020**, *12* (52), 57907-57915. DOI: 10.1021/acsami.0c18285.

(9) Han, Y.; Li, W.; Zhou, K.; Wu, X.; Wu, H.; Wu, X.; Shi, Q.; Diao, G.; Chen, M. Bimetallic Sulfide Co9S8/N-C@MoS2 Dodecahedral Heterogeneous Nanocages for Boosted Li/K Storage. *ChemNanoMat* **2019**, *6* (1), 132-138. DOI: 10.1002/cnma.201900601.

(10) Chen, W.; Hu, K.; Zheng, H.; Pan, Y.; Lv, Z.; Tu, X.; Zheng, C.; He, T.; Huang, F.; Dong, W. GeV(4) S(8) : a Novel Bimetallic Sulfide for Robust and Fast Potassium Storage. *Small* **2024**, e2311638. DOI: 10.1002/smll.202311638.

(11) Chen, X.; Cheng, N.; Zhang, L.; Xiang, G.; Ding, Y.-L.; Liu, Z. Flower-like spherical FeCoS2 coated by reduced graphene oxide as anode for high performance potassium ion storage. *J. Alloys Compd.* **2021**, *861*. DOI: 10.1016/j.jallcom.2020.158458.

(12) Hu, R.; Zhu, K.; Ye, K.; Yan, J.; Wang, Q.; Cao, D.; Wang, G. Influence of potential range selection on the SnS@C/rGO anodes in potassium ion battery. *Appl. Surf. Sci.* **2021**, *536*. DOI: 10.1016/j.apsusc.2020.147832.